SIAM J. Applied Dynamical Systems
Vol. 4, No. 2, pp. 282–311

Direct Chaotic Flux Quantification in Perturbed Planar Flows: General Time-Periodicity*

Sanjeeva Balasuriya†

Abstract. Chaotic flux occurring across a heteroclinic upon perturbing an area-preserving planar flow is examined. The perturbation is assumed to have general periodicity, extending the harmonic requirement that is often used. Its spatial and temporal parts are moreover not required to be separable. This scenario, though well-understood phenomenologically, has until now had no computable formula for the quantification of the resulting chaotic flux. This article derives such a formula, by directly assessing the unequal lobe areas that are transported via a turnstile mechanism. The formula involves a bi-infinite summation of quantities related to Fourier coefficients of the associated Melnikov function. These are themselves directly obtainable using a Fourier transform process. An example is treated in detail, illustrating the relative ease in which the flux computation can be performed using this theory.

Key words. chaotic flux, periodic perturbation, two-dimensional flow, lobe dynamics, Melnikov function

AMS subject classifications. 34C28, 37A25, 34C37, 37N10

DOI. 10.1137/040603243

1. Introduction.

This article is concerned with obtaining a computable quantification of the chaotic flux generated through perturbing an integrable planar system with a perturbation which has general time-periodicity. The specific setting will be stated first; a description of its contribution to the broader topic of quantifying chaotic flux will then be easier to present. The nearby area-preserving integrable flow shall be given by

$$\dot{x} = \mathrm{J}\,\nabla H(x), \tag{1.1}$$

where $x \in \Omega \subset \mathbb{R}^2$, $\mathrm{J} = \left(\begin{smallmatrix} 0 & -1 \\ 1 & 0 \end{smallmatrix}\right)$, and $H \in \mathrm{C}^2(\Omega)$ is the Hamiltonian function. It is assumed that (1.1) has a heteroclinic connection $\bar{x}(t)$ between two hyperbolic saddle points a and b (which need not be distinct). Thus, this heteroclinic is simultaneously a branch of the one-dimensional unstable manifold of a and the one-dimensional stable manifold of b. The regular phase-space structure precludes any complicated motion across this heteroclinic, which is therefore a flow separatrix.

The idea is to assess the chaotic flux across this separatrix under the influence of a perturbation to the velocity field in the form

$$\dot{x} = \mathrm{J}\,\nabla H(x) + \varepsilon\, h(x,t), \tag{1.2}$$

where the function $h : \Omega \times \mathbb{R} \to \mathbb{R}^2$ satisfies the following conditions:

*Received by the editors January 1, 2004; accepted for publication (in revised form) by J. Meiss August 12, 2004; published electronically April 14, 2005.
http://www.siam.org/journals/siads/4-2/60324.html
†School of Mathematics & Statistics, University of Sydney, NSW 2006, Australia (sanjeeva@maths.usyd.edu.au).

(a) For each fixed t, $h(x,t) \in \mathrm{C}^2(\Omega)$.
(b) For each fixed $x \in \Omega$, $h(x,t)$ as a function of $t \in \mathbb{R}$ is piecewise continuous, has well-defined left- and right-hand derivatives at all t, and is periodic with period $2\pi/\omega$.

Here, $0 < \varepsilon \ll 1$, and for nonzero ε the stable and unstable manifolds perturb, thereby presenting the possibility of chaotic transport occurring across the heteroclinic.

This problem has been solved quite comprehensively for the case where $h(x,t)$ is separable in the form $g(x)\,\theta(t)$, and the function $\theta(t)$ is harmonic. For the purposes of this paper *harmonic* will mean that $\theta(t) = \cos(\omega t - \beta)$ for a given frequency ω and phase β. In this case the perturbed manifolds intermingle regularly, creating lobes of equal area. One needs to define a "pseudoseparatrix" [35] for the perturbed flow, and it turns out that only specified lobes ("turnstiles") control transport across this pseudoseparatrix. It has been well known for some time that each lobe area is given by an integral (with appropriate limits) of a quantity called the Melnikov function [29, 31, 35, 28]. The Melnikov function is related to the signed distance between the perturbed stable and unstable manifolds [20, 4]. Many theoretical developments of lobe dynamics (some of which include effects of secondary manifold intersections, nonsmall ε, very small or very large ω, and nonharmonic θ) have evolved [28, 26, 31, 21, 27, 18, 8], yet as pointed out in [23] seldom provide methods of actually performing flux calculations. Indeed, such calculations have been numerically done using lobe dynamics only in a few specific cases [30, 21]. A theoretical, but computable, quantification of the flux using this idea in this time-harmonic separable setting was presented in [7, 6]. The former paper is a dynamically consistent approach to time-harmonically forced Euler flows, while the latter analyzes the best kinematical harmonic perturbation that could lead to increased chaotic flux.

Even within this separable setting, for θ not necessarily harmonic, a direct chaotic flux assessment is not available. In the various extensions to Melnikov theory in relation to transport [31, 12, 28, 10, 32, 11, 8], few concentrate on obtaining computable formulae quantifying the chaotic flux. Among the difficulties are defining a pseudoseparatrix and the fact that the lobes created need not have equal areas. Obtaining an expression for the chaotic flux from the lobe areas is also not obvious, since the lobes do not map to other lobes in as obvious a fashion as occurs in the harmonic case. The Melnikov function, which was itself harmonic and easily computed for harmonic θ (see [7]; see also Corollary 5.3), is no longer as tractable. This leaves no easy technique for calculating its integral, which is necessary in determining lobe areas. Though lobe area formulae are occasionally available in some settings (such as in [18] in which a mechanical Hamiltonian system is considered), there is normally no direct method of obtaining the chaotic flux in terms of fundamental quantities of the flow. In other words, although the process of chaotic transport via turnstile dynamics is well understood qualitatively, there is no method of *quantifying* the chaotic flux in a computable fashion.

This article will establish a method of directly quantifying the chaotic flux related to (1.2) under quite general conditions. The approach is interesting from both theoretical and computational perspectives. While providing an understanding of the role of Fourier modes of $h(\cdot,t)$ in the Melnikov development and flux computation, it illustrates an algorithm which is easy to implement. Importantly, the method requires neither harmonicity nor separability.

The problem as stated is one aspect of a global interest in quantifying transport in chaotic systems. Techniques such as Lyapunov exponents [20], effective diffusivities [5, 16, 3, 1, 15], width of stochastic layers [16, 3, 15], entropy and other measures on tracer distribution [17,

5, 26, 15], escape rates or transit times [17, 22, 25, 26, 14], asymptotic directionality [19], or intermaterial contact surfaces [2] are commonly used (see [23, 24, 15] for reviews). Many of these quantities are heuristically motivated and often need to be determined numerically or experimentally. It must be mentioned that these techniques, however, enjoy several advantages over the current approach: (i) they do not require a perturbative (i.e., near integrable) setting, (ii) separatrices (pseudo or otherwise) need not always be defined, and (iii) time-periodicity is not always necessary. Their shortcoming is that they often provide only indirect assessments (or diagnostics) of the chaotic flux, as opposed to the current approach, which quantifies the amount of phase-space area transported across a separatrix in unit time. This quantity is clearly by definition the *flux*. Although the current theory is limited by its perturbative and time-periodic nature, it is felt to be a substantial contribution, given the paucity of computable theoretical tools for direct definitions of flux.

This paper approaches the topic as follows. First, it is shown in section 2 that the Melnikov function can be obtained from $h(x,t)$ in terms of a filtering in Fourier space. This unusual (though not difficult) approach permits a quantification of the leading-order chaotic flux in terms of Fourier coefficients of $h(\cdot,t)$, certain properties of the unperturbed heteroclinic trajectory, and the zeros of the Melnikov function; this is presented in section 4. The flux formula has an infinite summation, but it will be argued that this usually converges rapidly. This formula can be evaluated relatively easily if the unperturbed flow is sufficiently well understood—a significant improvement on extant methods. The simplifications to the formula under a separability assumption on $h(x,t)$ are then presented in section 5, which also addresses several additional special cases for which simple formulae arise. In deriving all these flux formulae, an understanding of the appropriate pseudoseparatrices and turnstile structure for the general time-periodic case is necessary and is provided in section 3.

An example which has been used as a kinematical model for Rayleigh–Bénard convection is examined closely in section 6. The leading-order flux between cells is explicitly obtained for many different forms for $h(x,t)$. This includes square-wave-like time dependence, an instance in which $h(\cdot,t)$'s Fourier series has poor convergence, yet in which the flux computation is shown to converge rapidly. Illustrative computations are also performed for nonseparable h, for example, when h is generated from a traveling triangular wave. The flux computation is shown to converge quickly in a gross sense (to around two significant figures) in this instance, and more careful numerical investigation is presented on its detailed convergence. A general procedure for doing the leading-order flux calculation is a relatively easy exercise in comparison with other direct flux quantifying techniques, which may require numerical integration of the Melnikov function. Hence, the flux formula derived herein is a powerful tool in obtaining direct assessments of chaotic flux in near-integrable two-dimensional systems with general time-periodic perturbations.

2. Melnikov function. In computing the lobe areas in general, one usually takes the following approach. The heteroclinic manifold can be parametrized by $t \in \mathbb{R}$ by association with the point $\bar{x}(-t)$. The leading-order (signed) distance between the perturbed stable and unstable manifolds near a point t can be represented by [20, 4, 35]

$$\text{Distance} = \varepsilon \frac{M(t)}{|\nabla H(\bar{x}(-t))|} + \mathcal{O}(\varepsilon^2),$$

where $M(t)$ is called the Melnikov function, for which an expression will be presented shortly. More precisely, one first takes a specific "time-slice" of the $(2+1)$-dimensional phase-space of (1.2) and defines on this slice a Poincaré map which samples the flow every $2\pi/\omega$ time units. The fixed points a and b perturb but exist as fixed points of this Poincaré map, and these retain their stable and unstable manifolds with respect to this map. It is the signed distance between these perturbed manifolds, measured in the direction normal to the original heteroclinic manifold at the point $\bar{x}(-t)$, that the above distance expansion represents.

Given the periodicity hypothesis on $h(\cdot, t)$, it can be represented for each x in terms of a complex Fourier series

$$\frac{h(x,t^-)+h(x,t^+)}{2} = \sum_{n=-\infty}^{\infty} g_n(x)\, \exp(i\, n\, \omega\, t)\,,$$

where the functions $g_n : \Omega \to \mathbb{C}^2$ satisfy

$$g_n(x) = \frac{\omega}{2\,\pi} \int_0^{2\pi/\omega} h(x,t)\, \exp(-i\, n\, \omega\, t)\, \mathrm{d}t\,.$$

Define for each $n \in \mathbb{Z}$ the function $\lambda_n : \mathbb{R} \to \mathbb{C}$ by

$$\lambda_n(t) := \nabla H\left(\bar{x}(-t)\right) \cdot g_n\left(\bar{x}(-t)\right)\,.$$

Now, $\nabla H\left(\bar{x}(t)\right)$ exponentially decays to zero as $t \to \pm\infty$ given the hyperbolicity of the endpoints a and b. Since g_n is bounded on the closure of the heteroclinic manifold (it is continuous, and this set is compact), $\lambda_n \in \mathrm{L}^p(\mathbb{R})$ for any $p \in [1,\infty]$. This enables the definition of λ_n's Fourier transform

$$\hat{\lambda}_n(r) := \int_{-\infty}^{\infty} \lambda_n(t)\, \exp(-i\, r\, t)\, \mathrm{d}t,$$

which exists classically for all $n \in \mathbb{Z}$.

Proposition 2.1. *The Melnikov function $M(t)$ has a complex Fourier series representation*

$$M(t) = \sum_{n=-\infty}^{\infty} d_n\, \exp(i\, n\, \omega\, t)\,, \qquad \text{where} \quad d_n = \hat{\lambda}_n(n\,\omega)\,.$$

Proof. The Melnikov function associated with (1.2) is well known to be [20, 4, 35]

$$M(t) = \int_{-\infty}^{\infty} \nabla H\left(\bar{x}(\tau - t)\right) \cdot h\left(\bar{x}(\tau - t), \tau\right)\, \mathrm{d}\tau\,. \tag{2.1}$$

Utilizing $h(\cdot, t)$'s complex Fourier series,

$$\begin{aligned} M(t) &= \int_{-\infty}^{\infty} \sum_{n=-\infty}^{\infty} \nabla H\left(\bar{x}(\tau - t)\right) \cdot g_n\left(\bar{x}(\tau - t)\right) \exp(i\, n\, \omega\, \tau)\, \mathrm{d}\tau \\ &= \sum_{n=-\infty}^{\infty} \int_{-\infty}^{\infty} \lambda_n(t - \tau)\, \exp(i\, n\, \omega\, \tau)\, \mathrm{d}\tau \\ &= \sum_{n=-\infty}^{\infty} \exp(i\, n\, \omega\, t) \int_{-\infty}^{\infty} \lambda_n(\tau) \exp(-i\, n\, \omega\tau)\, \mathrm{d}\tau\,, \end{aligned}$$

from which the result follows. The dominated convergence theorem has been used to interchange the infinite summation and improper integral. ■

Remark 2.1. Since h is $(2\pi/\omega)$-periodic in t, this formulation shows that M must be as well.

Remark 2.2. If $h(\cdot,t)$ has a phase-shift (say, t is replaced by $t-\beta$), then M inherits the same phase-shift. Alternatively, if a shifted time parametrization is chosen for the heteroclinic trajectory $\bar{x}(t)$, then each λ_n has such a phase-shift, which again is inherited by M.

Remark 2.3. Since $\hat{\lambda}_n(r) \to 0$ as $r \to \pm\infty$ (by the Plancherel theorem $\hat{\lambda}_n$ is square integrable over $\mathbb{R}$ because λ_n is), this formulation also indicates that high frequencies present in $h(\cdot,t)$ undergo increased damping. Thus, the function $M(t)$ has muffled oscillations in comparison to $h(\cdot,t)$. This often results in $M(t)$ being smoother, and having fewer zeros, than $h(\cdot,t)$.

Remark 2.4. Trivial manipulations of the above can be used to represent $M(t)$ as a bi-infinite summation over the functions $\alpha_n(t)$, where $\alpha_n(t)$ is the convolution between the functions $\lambda_n(t)$ and $\exp(i\,n\,\omega\,t)$.

Remark 2.5. Expressing the Melnikov function in a Fourier series is not a new idea [14, 18]; determining formulae for its Fourier coefficients as done in Proposition 2.1, however, has not been done.

Lemma 2.2. *Suppose $h(x,t)$ is an even function in t for all $x \in \Omega$. Then, the Melnikov function's Fourier coefficients d_n satisfy*

$$d_n^* = d_{-n} \quad \text{for } n \in \mathbb{N},$$

where the star denotes the complex conjugate.

Proof. For even functions $h(\cdot,t)$, the complex Fourier coefficient functions $g_n(x) = g_{-n}(x)$ and are moreover real. Therefore, $\lambda_n(t) = \lambda_{-n}(t)$, which are also real functions. Using Proposition 2.1 for $n \in \mathbb{N}$,

$$d_{-n} = \hat{\lambda}_{-n}(-n\omega) = \left[\hat{\lambda}_{-n}(n\omega)\right]^* = \left[\hat{\lambda}_n(n\omega)\right]^* = d_n^*,$$

where the fact that $\hat{\lambda}^*(r) = \hat{\lambda}(-r)$ for any real r is used for real functions $\lambda(t)$. ■

3. Flux definition. This section will provide a rationalization for the chaotic flux definition, and establish its connection with the Melnikov function, for general periodic h. A discursive approach will be followed, since it is necessary to motivate the concept of the flux as a transfer of area per unit time. The flux mechanism is well understood in the standard instance in which $h(x,t)$ is both separable and harmonic. It helps to describe the transport mechanism in this case first; see also [29, 31, 35]. Some detail will need to be provided to understand Lemma 3.1, which extends the ideas to the present context.

Suppose then that $h(x,t) = g(x)\cos(\omega t - \beta)$, where β is a constant phase and $g : \Omega \to \mathbb{R}^2$. One can then use trigonometric identities [7, 6] to express

$$M(t) = |\hat{\gamma}(\omega)| \cos\{\omega t - \beta + \operatorname{Arg}[\hat{\gamma}(\omega)]\},$$

where $\gamma(t) = \nabla H(\bar{x}(-t)) \cdot g(\bar{x}(-t))$ (see also Corollary 5.3). Transverse zeros of M occur every π/ω, which correspond to transverse intersections between the perturbed stable and

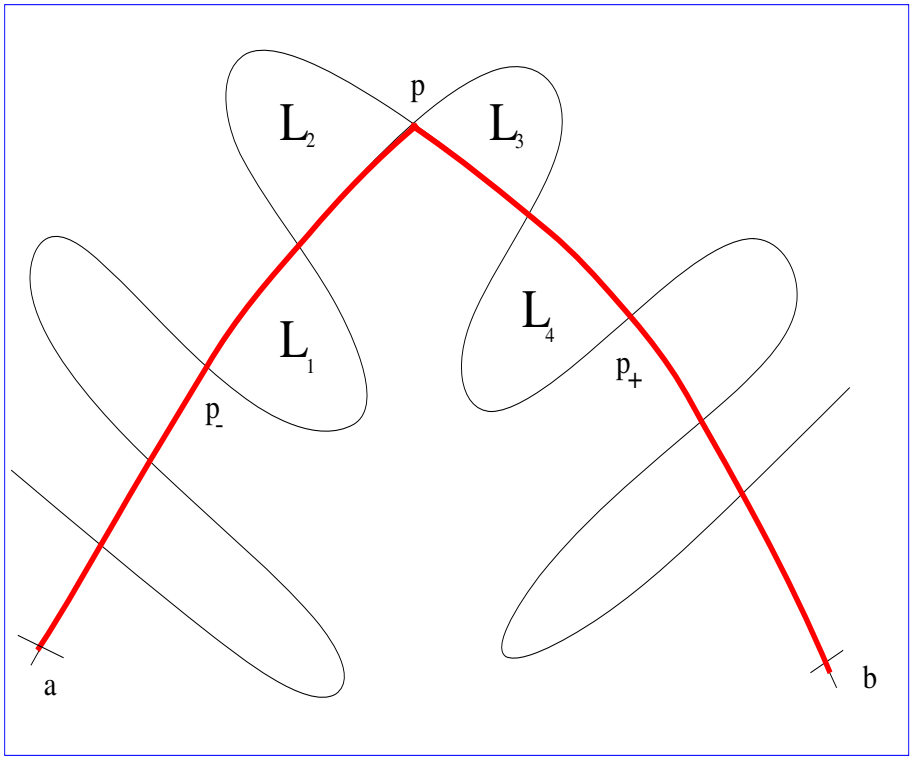

Figure 3.1. *Lobes and pseudoseparatrix (heavy red curve) for harmonic perturbations.*

unstable manifolds given that M represents the leading-order distance between these. Figure 3.1 shows this structure; a and b are the perturbed versions of the fixed points. What emerges is a *heteroclinic tangle* which is a signature of chaotic trajectories in its vicinity. Pick a *primary intersection point* [31, 29, 26, 35] between these manifolds and call it p. Define the *pseudoseparatrix* by combining the part of the unstable manifold of a, which lies between a and p, with the stable manifold of b, which lies between p and b; this is indicated with a heavy curve in the figure. This is $\mathcal{O}(\varepsilon)$-close to the original heteroclinic trajectory and will be used as the "boundary" across which flux is to be computed.

Upon iteration of the Poincaré map of period $2\pi/\omega$, the point p maps to p_+, and the point p_- maps to p. Notice that there are two distinct discrete heteroclinic orbits which exist in this perturbed case: one follows $\ldots, p_-, p, p_+ \ldots$, and the unlabeled set of manifold-intersection-points alternate with this set. By the $(2\pi/\omega)$-periodic Poincaré map, this means that the lobe L_1 maps to L_3, and L_2 maps to L_4 (it turns out that in this special case, all these lobes have the same area). If one thinks of what crosses the pseudoseparatrix per iteration of the Poincaré map, the area of L_1 crosses in one direction, whereas the area of L_2 crosses in the other. No other lobes cross the pseudoseparatrix, since they retain their relative positions with respect to the manifolds. This structure of four lobes L_1, L_2, L_3, and L_4 adjacent to the chosen primary intersection point p is called a *turnstile* [35]; the defining endpoints of the turnstile are the preimage and image of p (p_- and p_+, respectively) under the Poincaré map. The total area *exchanged* across the pseudoseparatrix per iteration of the Poincaré map can

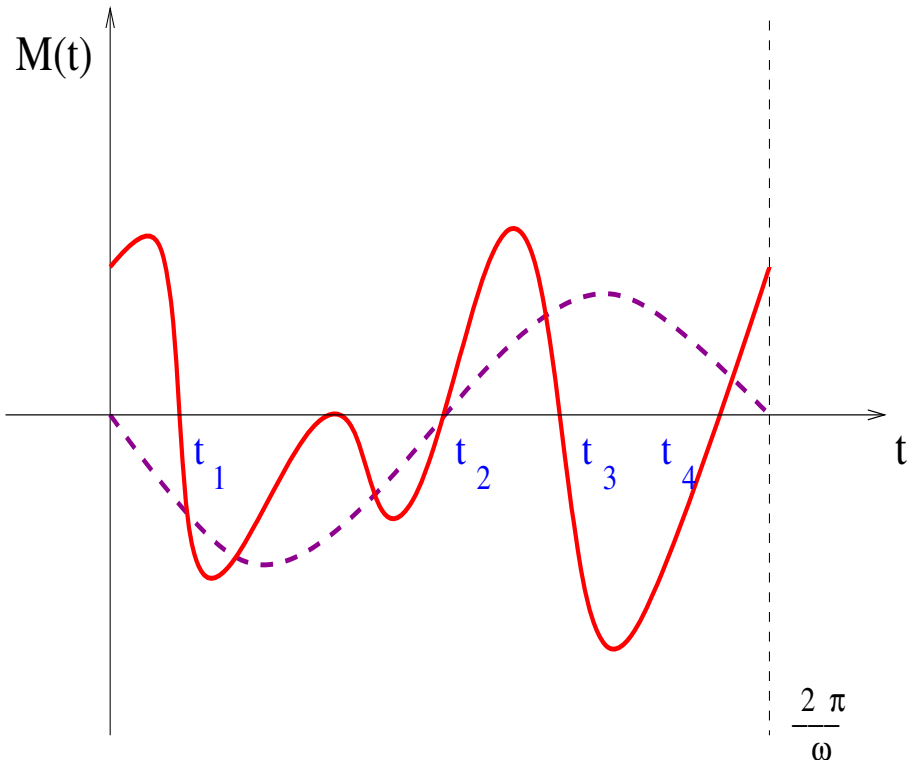

Figure 3.2. *Two Melnikov functions: Harmonic case (dashed purple curve) and a more general case (solid red curve).*

then be defined to be the sum of the areas of L_1 and L_2.

Now, if τ_1 and τ_2 are adjacent transverse zeros of the Melnikov function, then the lobe area (of the lobe defined with τ_1 and τ_2 as endpoints) is given by

$$\text{Area } = \varepsilon \int_{\tau_1}^{\tau_2} |M(t)| \, \mathrm{d}t + \mathcal{O}(\varepsilon^2) \, ;$$

see [29, 35]. In this case, the Melnikov function is harmonic and, modulo a shift, takes the form of the dashed curve in Figure 3.2. The two areas (one positive and the other negative) subtended by this dashed curve correspond to the two lobes L_1 and L_2 of Figure 3.1. Indeed, these areas are identical, since $M(t)$ takes the form $|\hat{\lambda}(\omega)| \cos(\omega t + \beta)$, the integral of whose absolute value between any two adjacent zeros is the same. This is so even if the spatial part of the perturbation g is *not* area-preserving, and is a consequence of harmonicity. The relevant area exchanged is the sum of these two areas, which can also be expressed as

$$\text{Area } = \varepsilon \int_{0}^{2\pi/\omega} |M(t)| \, \mathrm{d}t + \mathcal{O}(\varepsilon^2). \tag{3.1}$$

Most of what has been described so far in this section can be found in the literature for harmonic separable h [29, 35]. The next issue is the extension to general time-periodic functions of period $2\pi/\omega$, which are not necessarily separable. The corresponding Melnikov

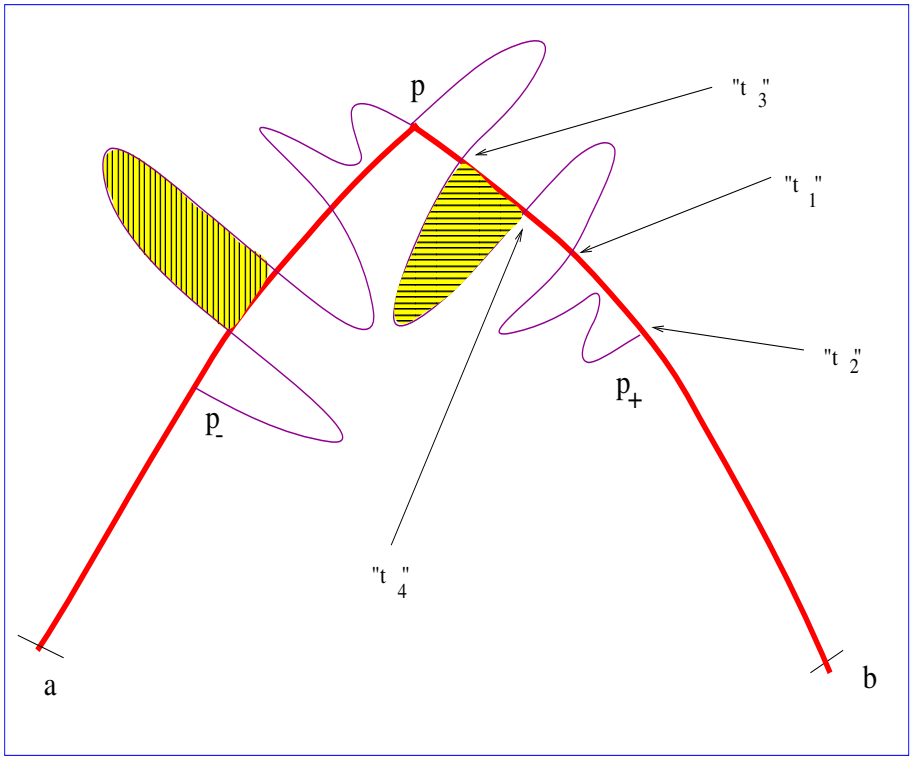

Figure 3.3. *Turnstile mechanism for the nonharmonic case.*

function, computed through Proposition 2.1, need not be harmonic. A possible form for $M(t)$ is illustrated as the solid curve in Figure 3.2. This particular example has four transverse zeros (which are labeled); notice also the presence of a nontransverse zero between t_1 and t_2. Now, since the Melnikov function corresponds to the leading-order signed distance between the perturbed stable and unstable manifolds associated with the Poincaré map of period $2\pi/\omega$, the Melnikov function does give important information on the topology of manifold intersections. If the solid curve in Figure 3.2 gives the Melnikov function, then Figure 3.3 illustrates a possible scenario for the manifold intersections—the Melnikov function is essentially repeatedly reproduced.

A subtle issue related to the presence of a nontransverse zero in the Melnikov function needs to be stated. Given that $M(t)$ provides only leading-order (in ε) information on the distance between manifolds, the presence of a nontransverse zero in $M(t)$ tells us nothing about intersections nearby. In this case, $\mathcal{O}(\varepsilon^2)$ terms are relevant in the distance function, and the nontransverse zero of M may be associated with either two, one, or no actual intersections between the manifolds. Thus, if nontransverse zeros exist, the Melnikov function is not necessarily topologically equivalent to the manifold intersections. This fact is irrelevant in the leading-order flux, since any lobes created through such higher-order effects have size $\mathcal{O}(\varepsilon^2)$.

In Figure 3.3, the situation where the nontransverse zero perturbs to no intersections is pictured. The points associated with t_1, t_2, t_3, and t_4 in the Melnikov function of Figure 3.2

are also indicated. A primary intersection point p has been chosen arbitrarily; in this case, it is the one corresponding to t_2 of the nonharmonic Melnikov function pictured in Figure 3.2. The fundamental turnstile is the set of lobes which lie between p_- (the preimage of p) and p_+ (its image). Lobes beyond this turnstile have not been pictured (these structures simply repeat). The pseudoseparatrix (displayed by a heavy curve) is as before; it is the portion of the unstable manifold of a lying between a and p, combined with the portion of the stable manifold of b lying between p and b. One lobe is vertically hatched in Figure 3.3; this maps to the horizontally hatched lobe upon iteration of the Poincaré map of period $2\pi/\omega$. The mapping behavior of the other lobes can also be deduced from this figure. Basically, *all* the lobes in the turnstile interchange their position with respect to the pseudoseparatrix. This argument shows that the amount of phase-space area which exchanges across the separatrix per iteration of the Poincaré map can therefore be expressed by (3.1) *even in this nonharmonic case.*

Since this occurs over a time of $2\pi/\omega$, one can *define* the chaotic flux by

$$\text{Flux} := \frac{\omega}{2\,\pi}\,[\text{Area exchanged across the pseudoseparatrix per iteration}]\ .$$

This is a common rationalization of the instantaneous chaotic flux [30, 7, 6], which incorporates the average amount of phase-space area transported per unit time. Since the lobe areas are $\mathcal{O}(\varepsilon)$, so is the flux. It can therefore be expanded in powers of ε as

$$\text{Flux } = \varepsilon\, s + \mathcal{O}(\varepsilon^2),$$

where s is the leading-order chaotic flux. Using this as a definition, the following has been argued.

Lemma 3.1. *In the case where the Melnikov function has $2m$ ($m \geq 1$) transverse zeros in each $(2\pi/\omega)$-period, the leading-order flux is given by*

$$s = \frac{\omega}{2\pi}\int_0^{2\pi/\omega} |M(t)|\ \mathrm{d}t.$$

Remark 3.1. The leading-order flux is the average value of the absolute value of the Melnikov function. A shift in the argument of M has no effect in evaluating this quantity.

Remark 3.2. By virtue of Remark 2.2, a phase-shift in $h(\cdot, t)$ or a different choice of time-zero of the heteroclinic $\bar{x}(t)$, does not affect the leading-order flux.

Remark 3.3. The Melnikov function must have an even number of transverse zeros in its fundamental period by topological considerations (it is periodic). If this number is zero, there is no consequent leading-order chaotic transport (though a channel-like nonchaotic mechanism [10, 32, 9] occurs).

Lemma 3.1 may be considered a definition of the leading-order chaotic flux related to mixing of fluid across the separatrix. This incorporates fluid exchange in both directions. One may be interested in the *directional flux* and require separate expressions for each direction. In order to quantify this, note that ∇H, which is orthogonal to the heteroclinic at all points, preserves its directionality with respect to the heteroclinic. Denote by s_+ the leading-order chaotic flux that is generated across the pseudoseparatrix in the direction defined by $+\nabla H$.

The analogous flux in the opposite direction shall be denoted s_-. Recall the sign convention: a positive Melnikov function corresponds to the vector drawn from the (perturbed) stable manifold to the unstable one having the same directionality as $+\nabla H$ [20]. Hence, the vertically hatched lobe in Figure 3.3 would correspond to a positive Melnikov function if ∇H were increasing in the *downward* direction. Notice that this lobe is in fact transferred in exactly the downward direction across the separatrix. On the other hand, if ∇H pointed in the upward direction in Figure 3.3, the lobe of interest would correspond to the Melnikov function being *negative*, and this lobe is then seen to transfer in the direction of $-\nabla H$.

Hence, lobes corresponding to positive M transfer in the direction of $+\nabla H$, whereas those with negative M transfer in the direction of $-\nabla H$. Upon defining the "positive part" and "negative part" functions,

$$[\xi]^+ = \begin{cases} \xi & \text{if } \xi > 0, \\ 0 & \text{if } \xi \le 0 \end{cases} \qquad \text{and} \qquad [\xi]^- = \begin{cases} -\xi & \text{if } \xi < 0 \\ 0 & \text{if } \xi \ge 0, \end{cases}$$

it is clear that the leading-order directional fluxes are then given by

$$s_\pm = \frac{\omega}{2\pi} \int_0^{2\pi/\omega} [M(t)]^\pm \, \mathrm{d}t \, .$$

The fluxes s_+ and s_- are equal for harmonic separable perturbations but not necessarily so in the general setting.

4. Flux formula. This section presents formulae for the flux and directional flux, in the case when $h(\cdot, t)$ has general time-periodicity (period $2\pi/\omega$), and need not be separable. This extends the results available in [7, 6].

Suppose that $M(t)$ has $2m$ transverse zeros in its fundamental period (it may have nontransverse zeros as well, but these play no part in what follows). Label these as t_j, $j = 0, 1, 2, \ldots 2m-1$, in an ordered fashion; since shifts in the Melnikov function's argument have no effect on the flux, one can choose any of the zeros to be t_0. This labeling creates $2m$ intervals; the jth ($j = 1, 2, \ldots 2m$) of these is $\mathrm{I}_j = (t_{j-1}, t_j)$. Let L_j be its length and T_j its midpoint. Define

$$\Xi_j = \begin{cases} 1 & \text{if } M(t) \ge 0 \text{ in } \mathrm{I}_j, \\ -1 & \text{if } M(t) \le 0 \text{ in } \mathrm{I}_j. \end{cases}$$

Note that Ξ_j is either $(-1)^j$ or $(-1)^{j+1}$ depending on the particular choice of t_0. The leading-order flux can then be expressed as an operation on the Fourier series of M, as follows (see also Corollary 1.2 in [18], in which a similar theme appears in a much more restrictive setting).

Theorem 4.1. *Suppose the Melnikov function $M(t)$ has complex Fourier coefficients $\{d_n\}$, and it also has $2m$ transverse zeros in each $2\pi/\omega$ period, where $m \ge 1$. Using the definitions above, the leading-order flux is then expressible as*

$$s = \sum_{n=-\infty}^{\infty} e_n, \qquad \textit{where} \quad e_0 = \frac{\omega \, d_0}{2\,\pi} \sum_{j=1}^{2m} \Xi_j \, L_j$$

$$\textit{and} \quad e_n = \frac{d_n}{\pi \, n} \sum_{j=1}^{2m} \Xi_j \exp\left(i \, n \, \omega \, T_j\right) \sin\left(\frac{n \, \omega \, L_j}{2}\right) \qquad \textit{for } n \ne 0.$$

Proof. The result of Lemma 3.1 gives

$$s = \frac{\omega}{2\pi} \sum_{j=1}^{2m} \int_{\mathrm{I}_j} \Xi_j M(t)\, \mathrm{d}t.$$

Replacing M with its Fourier series,

$$\begin{aligned} s &= \frac{\omega}{2\pi} \sum_{n=-\infty}^{\infty} d_n \sum_{j=1}^{2m} \Xi_j \int_{t_{j-1}}^{t_j} \exp\left(in\omega t\right)\, \mathrm{d}t \\ &= \sum_{n=-\infty, n\neq 0}^{\infty} \frac{d_n}{2\pi i n} \sum_{j=1}^{2m} \Xi_j \exp\left(in\omega t\right) \Big|_{t_{j-1}}^{t_j} + \frac{\omega\, d_0}{2\,\pi} \sum_{j=1}^{2m} \Xi_j \left(t_j - t_{j-1}\right). \end{aligned}$$

Now I_j has midpoint $T_j = \left(t_j + t_{j-1}\right)/2$ and length $L_j = t_j - t_{j-1}$, and so

$$\exp\left(in\omega t_j\right) - \exp\left(in\omega t_{j-1}\right) = 2\, i\, \exp\left(in\omega T_j\right) \sin\left(\frac{n\omega L_j}{2}\right),$$

and the result follows. ∎

Remark 4.1. An advantage to this formulation is that the Melnikov function need not be integrated—only its distribution of transverse zeros is necessary. The Fourier coefficients are also known directly from $d_n = \hat{\lambda}_n(n\omega)$. Any convenient phase-shift ϕ can also be used in the Melnikov function by virtue of Remark 3.2; this would correspond to the T_j's shifting by ϕ in addition to a rotation $\exp\left(in\omega\phi\right)$ being assessed in each d_n.

Remark 4.2. Theorem 4.1 gives the flux as an operation on the Fourier series of M: its Fourier coefficients need to be modulated by a quantity related its distribution of zeros, and then summed. Given that the d_n's (and consequently the e_n's) are damped for large $|n|$ because of the presence of $\hat{\lambda}_n(n\omega)$ (which decays as $n \to \pm\infty$), keeping only a few terms in this summation will often suffice. (This property is well illustrated in the example presented in section 6.)

Corollary 4.2. *Suppose the conditions for Theorem 4.1 are satisfied and moreover that $h(\cdot, t)$ is an even function. Then, following the notation of Theorem 4.1, $e_n^* = e_{-n}$ for $n \in \mathbb{N}$, and moreover*

$$s = e_0 + 2 \sum_{n=1}^{\infty} \mathrm{Re}\left(e_n\right).$$

Proof. Fix $n \in \mathbb{N}$. Since $h(\cdot, t)$ is even, it is known from Lemma 2.2 that the Melnikov function's Fourier coefficients satisfy $d_n^* = d_{-n}$. Using the definition for e_n given in Theorem 4.1,

$$\begin{aligned} e_{-n} &= -\frac{d_{-n}}{\pi n} \sum_{j=1}^{2m} \Xi_j \exp\left(-in\omega T_j\right) \sin\left(-\frac{n\omega L_j}{2}\right) \\ &= \frac{d_n^*}{\pi n} \sum_{j=1}^{2m} \Xi_j \exp\left(-in\omega T_j\right) \sin\left(\frac{n\omega L_j}{2}\right) \\ &= e_n^*. \end{aligned}$$

The expression for the leading-order flux is obtained by utilizing this in the bi-infinite summation of Theorem 4.1. ■

Proposition 4.3. *Suppose the Melnikov function $M(t)$ has complex Fourier coefficients $\{d_n\}$, and it also has $2m$ transverse zeros in each $2\pi/\omega$-period, where $m \geq 1$. The leading-order directional fluxes are then expressible as*

$$s_\pm = \sum_{n=-\infty}^{\infty} e_n^\pm, \qquad \textit{where} \quad e_0^\pm = \pm \frac{\omega\, d_0}{2\,\pi} \sum_{j=1}^{2m} [\Xi_j]^\pm \; L_j$$

$$\textit{and} \quad e_n^\pm = \pm \frac{d_n}{\pi\, n} \sum_{j=1}^{2m} [\Xi_j]^\pm \exp\left(i\, n\, \omega\, T_j\right) \sin\left(\frac{n\, \omega\, L_j}{2}\right) \qquad \textit{for } n \neq 0.$$

Proof. Using the definitions of section 3,

$$s_\pm = \frac{\omega}{2\,\pi} \sum_{j=1}^{2m} \int_{\mathrm{I}_j} [\Xi_j]^\pm \left(\pm\, M(t)\right)\, \mathrm{d}t\,.$$

Now simply mimic the proof of Theorem 4.1, noting that only the intervals corresponding to positive (or negative) M need to be summed over. ■

Remark 4.3. Let L_+ and L_- be the lengths of the partition of the fundamental interval $[0, 2\pi/\omega)$ in which M is, respectively, positive and negative. Then $e_0^\pm$ is given explicitly by

$$e_0^\pm = \pm \frac{\omega\, d_0\, L_\pm}{2\,\pi}\,.$$

Remark 4.4. If $d_0 = 0$, the Melnikov function has zero average, and hence $s_+ = s_- = s/2$. This could occur, for example, if the perturbation were either harmonic or area-preserving. If $d_0 \neq 0$, there is a *directional imbalance* in the flux which shall be defined by $\hat{s} := s_+ - s_-$.

Corollary 4.4. *Under the conditions of Proposition 4.3, the directional imbalance $\hat{s} := s_+ - s_-$ can be represented by*

$$\hat{s} = \sum_{n=-\infty}^{\infty} \hat{e}_n, \qquad \textit{where} \quad \hat{e}_0 = d_0 \quad \textit{and}$$

$$\hat{e}_n = \frac{d_n}{n\,\pi} \sum_{j=1}^{2m} \exp\left(i\, n\, \omega\, T_j\right) \sin\left(\frac{n\, \omega\, L_j}{2}\right) \qquad \textit{for } n \neq 0\,.$$

Proof. A straightforward subtraction of the expression for s_- from that for s_+ in Proposition 4.3 gives the result. ■

Considerable simplifications to the flux formula of Theorem 4.1 occur if the Melnikov function's transverse zeros are equally spaced. Such simplifications occur, for example, in the standard case of a harmonic separable perturbation [6, 7]; this case is additionally simple since $m = 1$ [7]. As shown through examples in section 6, equal spacing of zeros is likely to occur under less stringent conditions. If so, a "resonance" phenomenon emerges, as is apparent in the following result.

Proposition 4.5. *Suppose the Melnikov function has $2m$ equally spaced transverse zeros in each $2\pi/\omega$-period, where $m \geq 1$. Shift the Melnikov function such that $t = 0$ is a midpoint between two adjacent transverse zeros of M between which $M \geq 0$; let $\{d_n\}$ be the Fourier coefficients associated with this shifted M. Then, the leading-order fluxes are given by*

$$s = \frac{2}{\pi} \sum_{k=-\infty}^{\infty} \frac{(-1)^k \, d_{(2\,k+1)m}}{2\,k+1} \qquad \textit{and} \tag{4.1}$$

$$s_{\pm} = \frac{1}{\pi} \sum_{k=-\infty}^{\infty} \frac{(-1)^k \, d_{(2\,k+1)m}}{2\,k+1} \pm \frac{d_0}{2} \, .$$

Proof. For this choice of shift,

$$L_j = \frac{\pi}{\omega\, m} \quad , \quad T_j = \frac{j\,\pi}{\omega\, m} \quad , \quad \text{and} \quad \Xi_j = (-1)^j \, .$$

Using Theorem 4.1,

$$s = \sum_{n=-\infty, n\neq 0}^{\infty} \frac{d_n}{\pi n} \sum_{j=1}^{2m} (-1)^j \exp\left[in\omega\left(\frac{j\pi}{m\omega}\right)\right] \sin\left(\frac{n\omega}{2}\frac{\pi}{m\omega}\right) + \frac{\omega d_0}{2\pi} \sum_{j=1}^{2m} (-1)^j \frac{\pi}{\omega m} \, .$$

The final summation vanishes, and thus

$$s = \sum_{n=-\infty, n\neq 0}^{\infty} \frac{d_n}{\pi n} \sin\left(\frac{n\pi}{2m}\right) \sum_{j=1}^{2m} \left[-\exp\left(\frac{in\pi}{m}\right)\right]^j \, .$$

However,

$$\sum_{j=1}^{2m} \left[-\exp\left(\frac{in\pi}{m}\right)\right]^j = -\exp\left(\frac{in\pi}{m}\right) \frac{1-(-1)^{2m}\exp\left(2in\pi\right)}{1+\exp\left(\frac{in\pi}{m}\right)},$$

whose numerator vanishes. This term can therefore contribute only if its denominator vanishes as well, i.e., if $\exp\left(in\pi/m\right) = -1$, or if

$$\frac{n}{m} = 2k+1 \; ; \quad k \in \mathbb{Z}.$$

Therefore, the summation can be limited to the values where $n = (2k+1)m$ for integers k:

$$\begin{aligned} s &= \sum_{k=-\infty}^{\infty} \frac{d_{(2k+1)m}}{\pi(2k+1)m} \sin\left(\frac{(2k+1)\pi}{2}\right) \sum_{j=1}^{2m} (-1)^j \exp\left[i(2k+1)j\pi\right] \\ &= \sum_{k=-\infty}^{\infty} \frac{d_{(2k+1)m}}{\pi(2k+1)m} (-1)^k \sum_{j=1}^{2m} (-1)^j \, (-1)^j \, , \end{aligned}$$

from which the result for s follows. In order to compute s_+, note that one needs only to sum over even j intervals and follow exactly the same sort of argument as above; details will not be provided. The formula for s_- can then be obtained from $s_- = s - s_+$. ∎

Remark 4.5. For equally spaced zeros, it is only the Fourier coefficients n such that n/m is an integer and, moreover, is odd, which contribute to the leading-order (nondirectional) flux. The directional fluxes also require d_0—the Melnikov function's average value—but nothing else. Other coefficients have no effect whatsoever. For example, should $h(x,t)$ have a term of the form $p(x)\cos 2\omega t$ in its Fourier series, this does not contribute. The number of transverse zeros in M picks out only those frequencies $n\omega$ from $h(\cdot,t)$ which "resonate" in this specific sense.

Remark 4.6. This formula, and the resonance behavior, is essentially still valid even if M were not represented in this particular shifted form. More generally, d_n above would have an additional multiplicative factor of the form $\exp(in\omega\phi)$ associated with a phase shift ϕ. Care needs to be taken to ensure that *positive* areas are added, but the *odd* resonances are still the only ones which survive.

Remark 4.7. If $h(\cdot,t)$ has equally spaced zeros, the decays associated with the d_ns for large $|n|$ may result in M also having equally spaced zeros (this is since by Remark 2.3 higher oscillations are likely to be damped). This effect will be illustrated in the example in section 6.

5. Separable perturbation. The chaotic flux formulae are particularly easy to use if the perturbation is *separable*, i.e., if

$$h(x,t) = g(x)\,\theta(t),$$

where $g : \Omega \to \mathbb{R}^2$ is such that $g \in \mathrm{C}^2(\Omega)$, and $\theta : \mathbb{R} \to \mathbb{R}$ is $(2\pi/\omega)$-periodic, piecewise continuous, and has well-defined left- and right-hand derivatives at all t. Suppose that θ's complex Fourier coefficients are $\{c_n\}$, and define

$$\gamma(t) = \nabla H\left(\bar{x}(-t)\right) \cdot g\left(\bar{x}(-t)\right) .$$

The following preliminary results on the Melnikov function are easily obtainable.

Lemma 5.1. *The Melnikov function can be expressed as a convolution between γ and θ; i.e.,*

$$M(t) = \int_{-\infty}^{\infty} \gamma(t-\tau)\,\theta(\tau)\,d\tau = \int_{-\infty}^{\infty} \theta(t-\tau)\gamma(\tau)\,d\tau\,.$$

Proof. A direct application of the well-known equation (2.1) immediately gives the result. ∎

Lemma 5.2. *The Melnikov function has the complex Fourier representation*

$$M(t) = \sum_{-\infty}^{\infty} d_n \exp\left(i\,n\,\omega\,t\right), \qquad \textit{where} \quad d_n = c_n\,\hat{\gamma}\left(n\,\omega\right) .$$

Proof. One can use Lemma 5.1 directly, or notice that $g_n(x) = c_n\,g(x)$ in this case, and apply Proposition 2.1. ∎

Remark 5.1. The Fourier coefficient of M associated with a frequency $n\,\omega$ is obtained by combining the quantity of this frequency present in θ (c_n), with the "amount" of the same frequency available in γ ($\hat{\gamma}(n\omega)$).

Remark 5.2. One can think of obtaining $M(t)$ from $\theta(t)$ as a low-pass filter operation in the Fourier domain, since higher frequencies are damped more.

A direct application of Lemma 5.2 yields the known fact [30, 6, 7] that if θ is harmonic, then so is M with the same frequency ω. The following corollary gives additional information on how the modulus and the argument of the complex entity $\hat{\gamma}(\omega)$ affect the Melnikov function's amplitude and phase.

Corollary 5.3. *Suppose θ consists of only one harmonic, i.e., $\theta(t) = \cos(\omega t - \beta)$ for some constant β. Then the Melnikov function is itself harmonic and takes the form*

$$M(t) = |\hat{\gamma}(\omega)| \cos[\omega t - \beta + \operatorname{Arg}(\hat{\gamma}(\omega))] . \tag{5.1}$$

Proof. The complex Fourier coefficients of θ are $c_1 = (\cos\beta - i\sin\beta)/2 = (1/2)\exp(-i\beta)$ and $c_{-1} = (1/2)\exp(i\beta)$, and hence by Lemma 5.2,

$$\begin{aligned}
M(t) &= \frac{1}{2}\exp(-i\beta)\hat{\gamma}(\omega)\exp(i\omega t) + \frac{1}{2}\exp(i\beta)\hat{\gamma}(-\omega)\exp(-i\omega t) \\
&= \frac{1}{2}\hat{\gamma}(\omega)\exp(i\omega t - i\beta) + \left[\frac{1}{2}\hat{\gamma}(\omega)\exp(i\omega t - i\beta)\right]^* \\
&= 2\operatorname{Re}\left[\frac{1}{2}\hat{\gamma}(\omega)\exp(i\omega t - i\beta)\right] \\
&= \operatorname{Re}[\hat{\gamma}(\omega)]\cos[\omega t - \beta] - \operatorname{Im}[\hat{\gamma}(\omega)]\sin[\omega t - \beta] \\
&= |\hat{\gamma}(\omega)|\left\{\frac{\operatorname{Re}[\hat{\gamma}(\omega)]}{|\hat{\gamma}(\omega)|}\cos[\omega t - \beta] - \frac{\operatorname{Im}[\hat{\gamma}(\omega)]}{|\hat{\gamma}(\omega)|}\sin[\omega t - \beta]\right\} \\
&= |\hat{\gamma}(\omega)|\cos[\omega t - \beta + \operatorname{Arg}(\hat{\gamma}(\omega))] . \qquad \blacksquare
\end{aligned}$$

Remark 5.3. The form (5.1) is particularly easy to analyze. The Melnikov function has equally spaced zeros and a zero average and is trivial to integrate to determine lobe areas. See [6, 7].

Return once again to general periodic θ. The procedure for performing flux calculations is quite simple, since Lemma 5.2 shows that only *one* Fourier transform $\hat{\gamma}$ needs to be computed. It then needs to be sampled at the discrete values $n\omega$ to determine the Melnikov coefficients d_n. This is far simpler than the more general nonseparable instance of section 4, in which infinitely many Fourier transforms were necessary. Having determined the Melnikov function relatively easily, and having found its distribution of zeros, Theorem 4.1 can then be employed to compute the flux. An instance in which a direct formula for this flux is obtainable is presented in the following proposition.

Proposition 5.4. *Suppose $\theta(t) = a_0 + a_1\cos\omega t + b_1\sin\omega t$, for some real constants a_0, a_1, and b_1. If $|a_0\hat{\gamma}(0)| > |\hat{\gamma}(\omega)|\sqrt{a_1^2 + b_1^2}$, no chaotic flux results. If equality occurs, then there is*

no $\mathcal{O}(\varepsilon)$ chaotic flux. If $|a_0\hat{\gamma}(0)| < |\hat{\gamma}(\omega)|\sqrt{a_1^2+b_1^2}$, then the leading-order fluxes are

$$s = \frac{2}{\pi}\sqrt{(a_1^2+b_1^2)|\hat{\gamma}(\omega)|^2 - a_0^2\,|\hat{\gamma}(0)|^2} + \frac{2a_0\hat{\gamma}(0)}{\pi}\cos^{-1}\left(\frac{-a_0\hat{\gamma}(0)}{|\hat{\gamma}(\omega)|\sqrt{a_1^2+b_1^2}}\right) - a_0\hat{\gamma}(0)\,,$$

$$s_+ = \frac{1}{\pi}\sqrt{(a_1^2+b_1^2)|\hat{\gamma}(\omega)|^2 - a_0^2\,|\hat{\gamma}(0)|^2} + \frac{a_0\hat{\gamma}(0)}{\pi}\cos^{-1}\left(\frac{-a_0\hat{\gamma}(0)}{|\hat{\gamma}(\omega)|\sqrt{a_1^2+b_1^2}}\right), \quad \textit{and}$$

$$s_- = s_+ - a_0\,\hat{\gamma}(0)\,.$$

Proof. First, rewrite $\theta(t)$ as

$$\theta(t) = a_0 + \sqrt{{a_1}^2+{b_1}^2}\cos\left[\omega t+\beta\right]$$

for some phase angle β, and then set $\beta = 0$ since a phase-shift has no bearing on the final flux computation. Thus,

$$c_0 = a_0 \qquad \text{and} \qquad c_1 = \frac{\sqrt{{a_1}^2+{b_1}^2}}{2} = c_{-1}$$

with all other Fourier coefficients being zero. By Lemma 5.2, this leads to M's Fourier coefficients

$$\begin{aligned} d_0 &= a_0\int_{-\infty}^{\infty}\gamma(t)\,\mathrm{d}t = a_0\,\hat{\gamma}(0),\\ d_1 &= c_1\,\hat{\gamma}(\omega) = \frac{\sqrt{{a_1}^2+{b_1}^2}}{2}\,\hat{\gamma}(\omega), \quad \text{and}\\ d_{-1} &= c_{-1}\,\hat{\gamma}(-\omega) = \frac{\sqrt{{a_1}^2+{b_1}^2}}{2}\,\hat{\gamma}^*(\omega) = d_1^*, \end{aligned}$$

and with all unspecified d_ns vanishing. The Melnikov function is then

$$M(t) = a_0\hat{\gamma}(0) + 2\,\mathrm{Re}\left(d_1 e^{i\omega t}\right) = a_0\hat{\gamma}(0) + \sqrt{{a_1}^2+{b_1}^2}\,|\hat{\gamma}(\omega)|\cos\left[\omega\,(t-\phi)\right]$$

for some value $\phi(\omega, a_1, b_1)$ (see the proof of Corollary 5.3 if additional details of this reformulation are required). Set $\phi = 0$ to define a new Melnikov function

$$M(t) = a_0\hat{\gamma}(0) + \sqrt{{a_1}^2+{b_1}^2}\,|\hat{\gamma}(\omega)|\,\cos\omega t,$$

where $M(t)$ is retained by an abuse of notation. (Recall that a phase-shift in M also does not affect the leading-order flux.) While d_0 does not change, now $d_1 = d_{-1} = \sqrt{{a_1}^2+{b_1}^2}\,|\hat{\gamma}(\omega)|/2$. Transverse zeros are only permissible if

$$|a_0\,\hat{\gamma}(0)| < \sqrt{{a_1}^2+{b_1}^2}\;|\hat{\gamma}(\omega)|\,,$$

in which case two such zeros exist (and so $m = 1$). In the event that equality occurs above, there are two *nontransverse* zeros, and the leading-order flux is therefore zero (the actual flux may not be zero, but it will be of higher order). Given the evenness of the new Melnikov function, it is convenient here to think of the base interval as $[-\pi/\omega, \pi/\omega)$. There are only two intervals of interest here: $M > 0$ in an interval of length L_+ with midpoint $T_+ = 0$ and $M < 0$ in an interval of length $L_- = 2\pi/\omega - L_+$ centered at $T_- = -\pi/\omega$. Here,

$$L_+ = \frac{2}{\omega} \cos^{-1}\left(\frac{-a_0 \hat{\gamma}(0)}{\sqrt{{a_1}^2 + {b_1}^2}\, |\hat{\gamma}(\omega)|} \right).$$

Substituting into the flux formula of Theorem 4.1,

$$\begin{aligned} s &= \frac{d_1}{\pi}\left[\sin\left(\frac{\omega L_+}{2}\right) - e^{-i\pi}\sin\left(\frac{\omega}{2}\left[\frac{2\pi}{\omega} - L_+\right]\right)\right] \\ &\quad + \frac{d_{-1}}{-\pi}\left[-\sin\left(\frac{\omega L_+}{2}\right) - e^{i\pi}\sin\left(-\frac{\omega}{2}\left[\frac{2\pi}{\omega} - L_+\right]\right)\right] + \frac{\omega d_0}{2\pi}\left[L_+ - \left(\frac{2\pi}{\omega} - L_+\right)\right] \\ &= \frac{4\, d_1}{\pi}\sin\left(\frac{\omega L_+}{2}\right) + \frac{\omega\, d_0\, L_+}{\pi} - d_0. \end{aligned}$$

However,

$$\sin\left(\frac{\omega L_+}{2}\right) = \frac{\sqrt{\left({a_1}^2 + {b_1}^2\right)|\hat{\gamma}(\omega)|^2 - a_0^2\,|\hat{\gamma}(0)|^2}}{\sqrt{{a_1}^2 + {b_1}^2}\,|\hat{\gamma}(\omega)|},$$

and substitution yields the formula for s. In computing s_+, notice that all terms which have the term $[2\pi/\omega - L_+]$ can be omitted from the calculation used for s, and the result is easily obtained. Once again, s_- is calculated by subtracting s_+ from s. ■

Remark 5.4. The directional imbalance in instantaneous flux transfer in this case is given by

$$\hat{s} := s_+ - s_- = a_0\, \hat{\gamma}(0) = a_0 \int_{-\infty}^{\infty} \nabla H\left(\bar{x}(t)\right) \cdot g\left(\bar{x}(t)\right)\, \mathrm{d}t\,.$$

Corollary 5.5. *Suppose $\theta(t) = a_1 \cos\omega t + b_1 \sin\omega t$. The directional chaotic fluxes s_+ and s_- are equal, and the leading-order chaotic flux is*

$$s = \frac{2}{\pi}\,|\hat{\gamma}(\omega)|\,\sqrt{a_1^2 + b_1^2}\,.$$

Proof. Simply set $a_0 = 0$ in the result of Proposition 5.4. ■

This result is consistent with that previously obtained in [7, 6], in which the leading-order flux is proportional to a modulus of a Fourier transform. It can also be directly obtained by integrating the harmonic Melnikov function that can be derived using Corollary 5.3. If the harmonic $\theta(t)$ of Corollary 5.5 is perturbed slightly with a small vertical shift a_0, the flux turns out to increase, as given below.

Corollary 5.6. *Suppose θ is as given in Proposition 5.4, and moreover $|a_0| \ll \sqrt{a_1^2 + b_1^2}$. Then the leading-order flux is*

$$s = \frac{2}{\pi} |\hat{\gamma}(\omega)| \sqrt{a_1^2 + b_1^2} + a_0^2 \left(\frac{|\hat{\gamma}(0)|^2}{\pi |\hat{\gamma}(\omega)| \sqrt{a_1^2 + b_1^2}} \right) + \mathcal{O}\left(\frac{a_0^4}{(a_1^2 + b_1^2)^2} \right).$$

Proof. A straightforward Taylor expansion does the trick but will be skipped. ∎

6. An example. An example which has been used as a kinematical model for Rayleigh–Bénard convection [13, 33, 34] will be considered. This model has also been analyzed in a variety of different instances from a dynamical systems perspective [3, 7, 6, 1]. In this section, (x, y) represent rectangular coordinates in $\mathbb{R}^2$. The unperturbed flow is

$$\dot{x} = -\sin(2\pi x)\sin(2\pi y), \qquad \dot{y} = -\cos(2\pi x)\cos(2\pi y),$$

for which $H(x, y) = -\sin(2\pi x)\cos(2\pi y)/(2\pi)$ serves as a Hamiltonian. The phase space structure is that of a periodic lattice of square cells of alternating rotation, as shown in Figure 6.1. The chaotic flux occurring across the heteroclinic trajectory indicated with a heavy blue line in Figure 6.1 will be assessed, under the influence of a time-periodic perturbation. As can be seen, this measures the leading-order intercellular transport. It can be shown [7, 6, 3] that for the symmetric time-parametrization along this heteroclinic, $\bar{x}(t) \equiv 0$ and

$$\bar{y}(t) = \begin{cases} \frac{1}{2\pi} \cos^{-1}[-\operatorname{sech}(2\pi t)] & \text{if } t \le 0, \\ 1 - \frac{1}{2\pi} \cos^{-1}[-\operatorname{sech}(2\pi t)] & \text{if } t > 0. \end{cases}$$

This enables ∇H to be expressed along the heteroclinic by

$$\nabla H(\bar{x}(t), \bar{y}(t)) = (\operatorname{sech}(2\pi t), 0).$$

Now imagine perturbing the vector field $\mathrm{J}\nabla H$ through the addition of the time-periodic perturbation $\varepsilon h(x, t)$. Seven different forms for h will be considered, essentially in order of increasing complexity, in order to highlight the roles of nonharmonicity and nonseparability.

6.1. Case (i). Begin with the simplest case in which the perturbation is separable and its spatial part is trivial. That is, $h(x, t) = g(x)\theta(t)$, in which g is constant. Following the notation of section 5,

$$\gamma(t) = [\nabla H \cdot g](\bar{x}(-t), \bar{y}(-t)) = K \operatorname{sech}(2\pi t)$$

for some real constant K (assumed nonzero). The Fourier transform of $\gamma(t)$ is

$$\hat{\gamma}(\omega) = \frac{K}{2} \operatorname{sech}\left(\frac{\omega}{4}\right).$$

If θ is $(2\pi/\omega)$-periodic with Fourier coefficients $\{c_n\}$, Lemma 5.2 tells us that the Fourier coefficients of the Melnikov function are

$$d_n = \frac{K c_n}{2} \operatorname{sech}\left(\frac{n\omega}{4}\right).$$

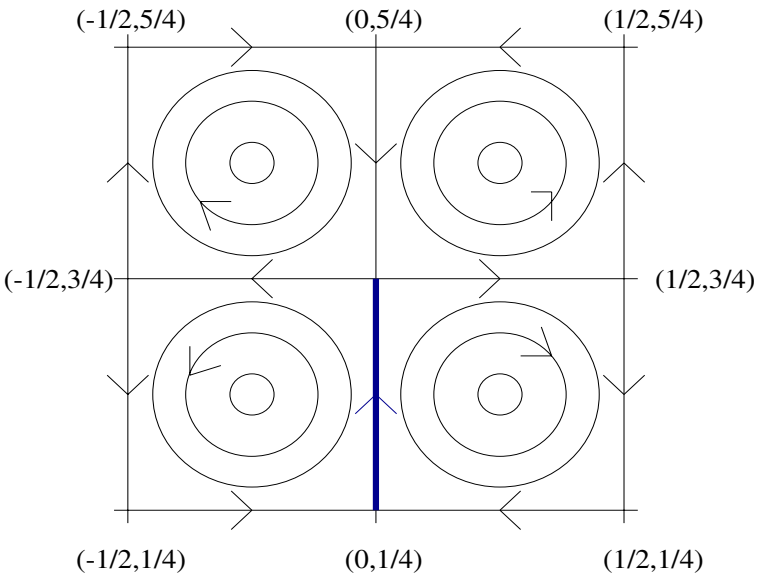

Figure 6.1. *Phase-space for the unperturbed flow of section 6.*

The computations in this instance will focus on the case in which θ contains only one mode plus a constant term, as given in Proposition 5.4. The leading-order flux is then

$$s = \frac{|K|}{\pi}\sqrt{(a_1^2+b_1^2)\operatorname{sech}^2\frac{\omega}{4} - a_0^2} + \frac{K}{2}\left[\frac{2a_0}{\pi}\cos^{-1}\left(\frac{-a_0\,|K|\cosh\frac{\omega}{4}}{K\sqrt{a_1^2+b_1^2}}\right) - a_0\right]$$

providing the argument of the first square-root above is positive. A sufficient condition for chaotic transport is therefore that

$$\omega < 4\operatorname{sech}^{-1}\frac{|a_0|}{\sqrt{a_1^2+b_1^2}}\,, \tag{6.1}$$

which relates the frequency with the ratio of the amplitudes of the constant and harmonic terms. Thus, chaotic transport will always occur for small enough frequencies for perturbations of this sort. For investigation of the flux within this regime, adopt the attitude that the amplitude of the modal term in θ (i.e., $\sqrt{a_1^2+b_1^2}$) is fixed, as is K, and investigate the flux variation with respect to the control parameters a_0 and ω, which relate to vertical translation and horizontal compression of the graph of θ. This behavior is illustrated in Figures 6.2 and 6.3. In each case, the abrupt end to the curves represents the transition in which s becomes complex, corresponding to the Melnikov function failing to have a transverse zero. If so (and this corresponds to the inequality (6.1) reversing), a nonchaotic channel-like transport occurs between cells [10, 9, 32]. In the chaotic regime, Figure 6.2 shows the flux variation as a function of the frequency. If $a_0 \neq 0$, it is apparently increasing as a function of ω for frequencies near this bifurcation. Choosing higher values of a_0 causes the curves to shift upward. If, however,

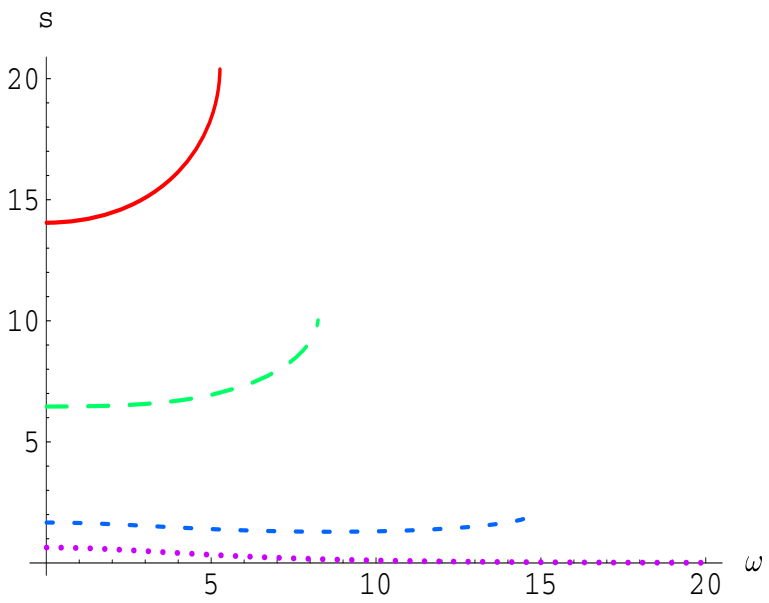

Figure 6.2. *Behavior of s as a function of ω for case* (i): $a_1 = 2$, $b_1 = 0$, *and* $K = 1$. *The curves are* $a_0 = 1$ *(solid red curve),* $a_0 = 0.5$ *(long green dashes),* $a_0 = 0.1$ *(short blue dashes), and* $a_0 = 0$ *(purple dots).*

$a_0 = 0$, then the flux is well defined and decreasing in ω for all ω (and indeed behaves like sech $(\omega/4)$), as shown in the dotted curve in Figure 6.2. In Figure 6.3, the flux variation with a_0 is displayed for three different ω's. For small a_0, smaller frequencies generate more flux in a marginal sense—an effect which reverses substantially for larger a_0.

The directional fluxes $s_\pm$ possess very similar qualitative behavior to s in this case. The directional imbalance is $\hat{s} = a_0 K/2$. If $a_0 K > 0$, there is more flux transferred from left to right across the heavy line in Figure 6.1.

6.2. Case (ii). Within the constant g ansatz, consider a more general instance where θ has infinitely many modes. Take the $(2\pi/\omega)$-periodic square wave which in a base period is defined by

$$\theta(t) = \begin{cases} 1 & \text{if } 0 < t < \frac{\pi}{2\omega} \text{ or } \frac{3\pi}{2\omega} < t < \frac{2\pi}{\omega}, \\ -1 & \text{if } \frac{\pi}{2\omega} < t < \frac{3\pi}{2\omega}. \end{cases}$$

This has Fourier coefficients

$$c_0 = 0 \quad \text{and} \quad c_n = \frac{1-(-1)^n}{n\,\pi} \sin\frac{n\,\pi}{2} \quad \text{for } n \neq 0.$$

Now M is continuous and also has period $2\pi/\omega$. By Proposition 2.1, its Fourier coefficients are

$$d_0 = 0 \quad \text{and} \quad d_n = \left(\frac{K}{2}\right) \frac{1-(-1)^n}{n\pi} \operatorname{sech}\frac{n\omega}{4} \sin\frac{n\pi}{2} \quad \text{for} \quad n \neq 0.$$

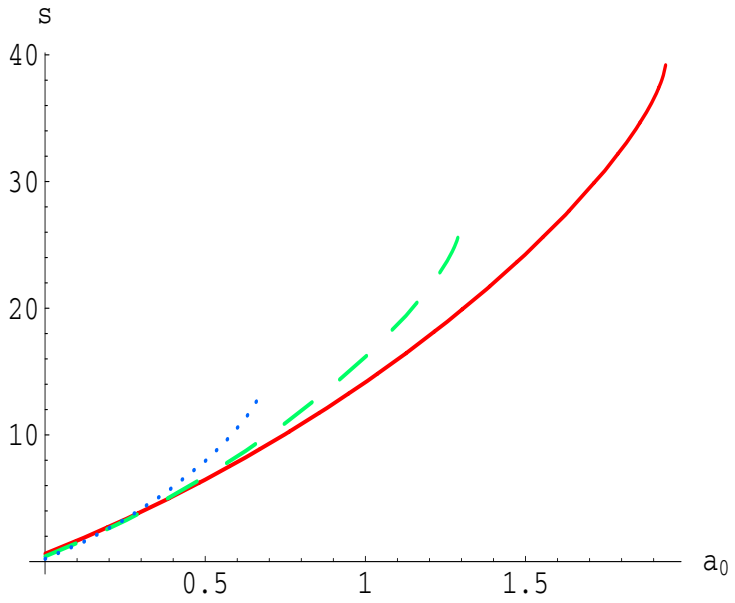

Figure 6.3. *Behavior of s as a function of a_0 for case* (i): $a_1 = 2$, $b_1 = 0$, *and* $K = 1$. *The three curves are* $\omega = 1$ *(solid red curve),* $\omega = 4$ *(dashed green curve), and* $\omega = 7$ *(dotted blue curve).*

Using this, it is possible to express M as

$$M(t) = \frac{2\,K}{\pi} \sum_{j=1}^{\infty} \frac{(-1)^{j+1}}{2\,j-1} \operatorname{sech}\left[\frac{(2j-1)\,\omega}{4}\right] \cos\left[(2j-1)\,\omega t\right],$$

which clearly has zeros at $t = \pi/(2\omega)$ and $t = 3\pi/(2\omega)$ within the domain $[0, 2\pi/\omega)$. A numerically generated sketch of $M(t)$ with the choice $\omega = \pi$ and $K = 1$ is shown in Figure 6.4, confirming that these are the only zeros. The dashed curve in this figure is the graph obtained by just keeping the $j = 1$ term, illustrating the quick convergence behavior. In fact, keeping about seven terms in the summation appears to guarantee six-digit accuracy, in spite of the fact that θ has slow convergence in its Fourier series. To use the formula of Theorem 4.1, there are only two intervals that one needs to consider. If $K > 0$, the midpoints and lengths are given by $T_+ = 0$, $L_+ = \pi/\omega$, $T_- = \pi/\omega$, and $L_- = \pi/\omega$, where the positive (resp., negative) subscript refers to whether M is positive (resp., negative) in that particular interval. If $K < 0$, the subscripts need to be reversed, which will be compensated for in the final result by using an appropriate absolute value. Using Theorem 4.1, the quantities

$$e_0 = 0 \quad \text{and} \quad e_n = \frac{d_n}{\pi\, n}\left[1 - (-1)^n\right] \sin\frac{n\,\pi}{2} \quad \text{for} \quad n \neq 0$$

are obtained. Notice that these are real. Since $\theta(t)$ is an even function, Corollary 4.2 is applicable, and moreover since all even n terms in e_n vanish because of the nature of the sequence,

$$s = 2 \sum_{j=1}^{\infty} e_{2j-1}\,.$$

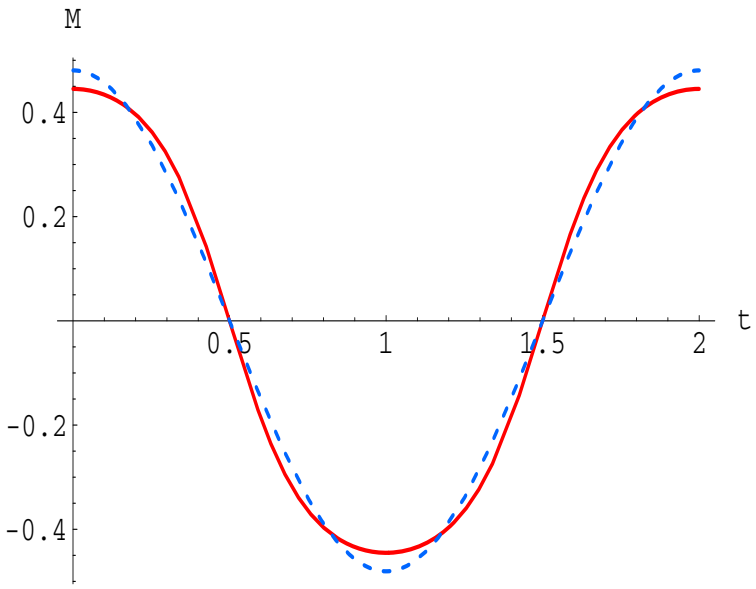

Figure 6.4. *The Melnikov function (solid red curve) and its single harmonic approximation (dashed blue curve) for case* (ii) *with* $K = 1$ *and* $\omega = \pi$.

The vanishing of the even terms is consistent with the "resonance" behavior expected from Proposition 4.5, since the zeros of the Melnikov function are evenly spaced in this instance. Substitution and simplification lead to the exact expression

$$s = \frac{4\,|K|}{\pi^2} \sum_{j=1}^{\infty} \frac{1}{(2j-1)^2} \operatorname{sech}\left(\frac{(2j-1)\,\omega}{4}\right),$$

whose rapid convergence means that it can be approximated easily with just a few terms.

6.3. Case (iii). An instance in which numerical evaluation is necessary is now presented. Suppose g remains constant as before, but now

$$\theta(t) = \sin(\pi t) - 3\cos(2\pi t) + 4\cos(3\pi t) + \frac{1}{2}\sin(23\pi t),$$

which is shown in its fundamental domain $[0, 2)$ by the dashed curve in Figure 6.5. Here, $\omega = \pi$. The corresponding Melnikov function, computed via Fourier coefficients in the usual fashion, is also displayed in this figure (where $K = -5$ is chosen for variety). The Melnikov function has only four zeros, as opposed to θ, which has eight. It is also smoother than θ, from which it is derived using a low-pass filtering (see Remarks 2.3 and 5.2). One can numerically compute the zeros of M (which turn out to be 0.249415, 0.819345, 1.25022, and 1.55607 to six significant figures, independent of the choice made for K) and thereby determine the midpoints T_j and the lengths L_j of the four intervals. Since one knows the d_ns, Theorem 4.1 can now be used to determine the leading-order flux s. There are only eight nonzero values for the e_n's in Theorem 4.1, and upon doing the arithmetic, one obtains $s = 0.463583\,|K|$. If

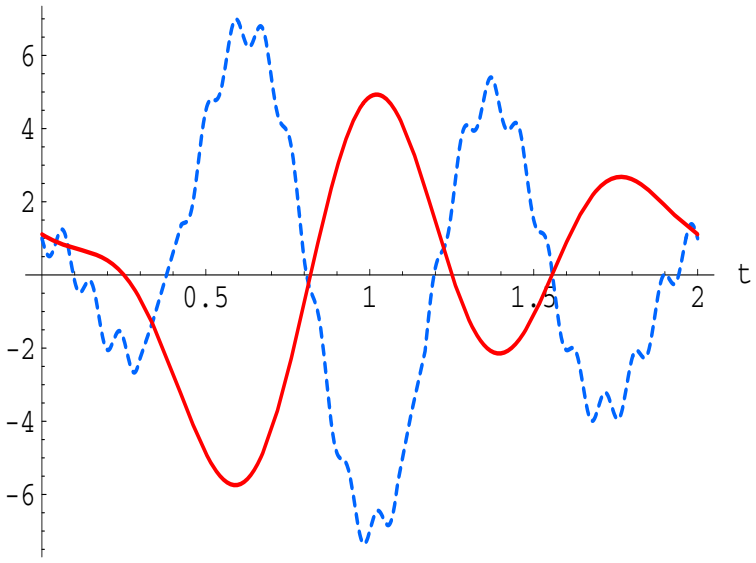

Figure 6.5. *The function θ (dashed blue curve) and its corresponding Melnikov function (solid red curve) with the choice $K = -5$ for case* (iii).

necessary, this value can be expressed to a much higher degree of accuracy quite easily, since the computations involve mainly the determination of the roots of $M(t)$ which can be done to as high a degree of accuracy as required. Since M has average value zero, the directional leading-order fluxes are equal in this case.

6.4. Case (iv). The constraint that g be constant is now removed. Suppose that the flow is derived from perturbing the original Hamiltonian $H(x, y)$ with the additive term

$$H_1(x, y, t) = \varepsilon \frac{1}{2\pi} \left[\sin(2\pi y) - \sin(2\pi x)\right] \cos(\omega t + \beta),$$

where β is a constant phase. This is the identical perturbation addressed using a "separatrix map" in section VI in [1]. Since the phase β can be ignored, this has only a single harmonic $\theta(t) = \cos(\omega t)$. The corresponding spatial function $g(x, y)$ is equal to $(-\cos 2\pi y, -\cos 2\pi x)$ and is not a constant. Therefore,

$$\gamma(t) = -\cos(2\pi \bar{y}(-t)) \operatorname{sech}(-2\pi t) = \operatorname{sech}^2(2\pi t),$$

whose Fourier transform is

$$\hat{\gamma}(\omega) = \frac{\omega}{4\pi} \operatorname{cosech}\left(\frac{\omega}{4}\right).$$

From Corollary 5.3, the Melnikov function, modulo a shift in t, takes the form

$$M(t) = \frac{\omega}{4\,\pi} \operatorname{cosech}\left(\frac{\omega}{4}\right) \cos(\omega\, t)\ .$$

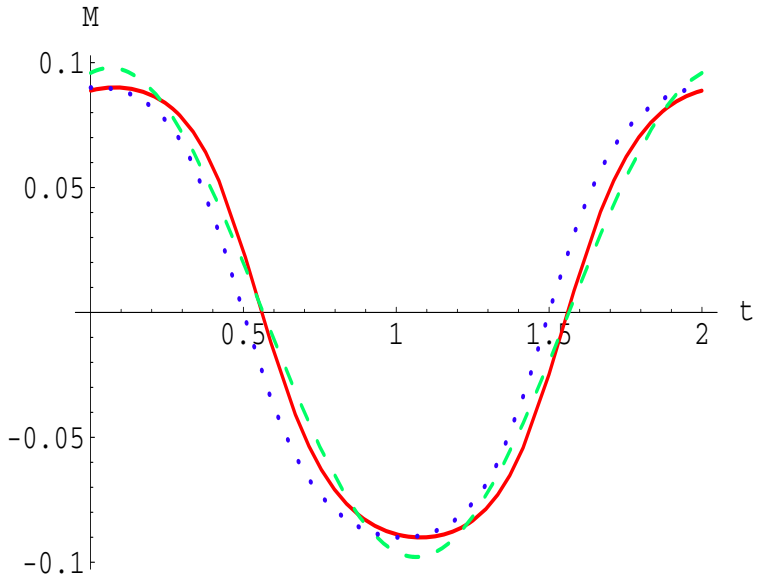

Figure 6.6. *The Melnikov function (solid red curve), its single harmonic approximation (dashed green curve), and the shifted Melnikov function (dotted blue curve) for case* (v).

The flux is also computable via a direct application of Corollary 5.5,

$$s = \frac{\omega}{2\pi^2}\,\text{cosech}\left(\frac{\omega}{4}\right),$$

which is a straightforward result given the harmonic nature of the perturbation.

6.5. Case (v). Now choose a more complicated perturbation while still remaining within the separable ansatz. It is only the x-component of $g(0,y)$ that contributes to $\gamma(t)$; take this to be the function $g^x(0,y) = y$. Therefore,

$$\gamma(t) = \bar{y}(-t)\,\text{sech}\,(-2\pi t)\,,$$

whose Fourier transform is no longer easily expressed and requires numerical evaluation. Take θ to be the square wave analyzed in case (ii), but choose $\omega = \pi$. The Fourier transform $\hat{\gamma}$ needs to be numerically obtained, and this was done using Mathematica's Fourier transform software. Now, θ's Fourier coefficients c_n are as given in case (ii), and one can compute $d_n = c_n\hat{\gamma}\,(n\pi)$ numerically. These Fourier coefficients of M are seen to satisfy the conditions $d_n = 0$ for even n (since c_n has this property) and $d_n = d^*_{-n}$ for odd n (since θ is even and Lemma 2.2 applies). This enables the Melnikov function to be written in the form

$$M(t) = 2\sum_{j=1}^{\infty} |d_{2j-1}|\,\cos\left[(2j-1)\,\pi t + \text{Arg}\,(d_{2j-1})\right],$$

whose numerically generated sketch appears in Figure 6.6 as the solid curve. Once again, it is seen that quick convergence is obtained; keeping only the $j = 1$ term gives the single harmonic

approximation shown by the dashed curve. The zeros are located at $t = 0.5602496185$ and 1.5602496185 and are to this order of accuracy equally spaced. There is hardly any qualitative difference in this Melnikov function and that pictured in Figure 6.4, for which g was constant. It may be that the same topological intersection pattern would result for monotone g, in keeping with the speculation in [6]. The Melnikov function can be shifted by multiplying each d_n by $\exp(0.0602496185\, i\, n\, \pi)$ such that the new Melnikov function now satisfies the shift for which Proposition 4.5 is applicable. The resulting shifted Melnikov function is illustrated in Figure 6.6 as the dotted curve. Proposition 4.5 can now be directly used to calculate the flux, with the shifted d_ns as the coefficients, and with $m = 1$. Applying the simple formula using 15 nonzero terms in the infinite summation gives the value $s = 0.064360176$. This value appears to be accurate to eight significant digits in that no changes in these digits were observed when increasing the number of terms in the summation.

6.6. Case (vi). The separability assumption on h is now relaxed. Note that it is only the x-component of h which contributes to the λ_n functions, since ∇H is purely in the x-direction. Suppose now that this component, h^x, is given by

$$h^x(x, y, t) = \cos[4\,\pi\,(y - t)] + 2\,\sin[3\,\pi\,(x - 2\,t)]\ .$$

This is a combination of a horizontal traveling wave and a vertical traveling wave with unequal speeds. The perturbation has period 1, corresponding to $\omega = 2\,\pi$. In the Fourier expansion

$$h^x(x, y, t) = \sum_{n=-\infty}^{\infty} g_n^x(x, y)\,\exp(i\, n\, 2\,\pi\, t)\,,$$

the only terms which survive are

$$g_{\pm 2}^x(x, y) = \frac{1}{2}\exp(\mp i\, 4\,\pi\, y)\,, \qquad g_{\pm 3}^x(x, y) = \exp(\pm\, i\, 3\,\pi\, x)\ .$$

The corresponding λ_n are

$$\lambda_{\pm 2}(t) = \frac{1}{2}\mathrm{sech}\,(2\pi t)\left[2\mathrm{sech}^2\,(2\pi t) - 1\right] \pm i\,\mathrm{sech}^2\,(2\pi t)\tanh(2\pi t)\,,\ \ \lambda_{\pm 3}(t) = \pm i\,\mathrm{sech}\,(2\pi t)\ .$$

Mathematica can be employed to compute the associated Fourier transforms

$$\hat{\lambda}_{\pm 2}(r) = \frac{r^2}{16\,\pi^2}\left[\mathrm{sech}\left(\frac{r}{2}\right) \pm \mathrm{cosech}\left(\frac{r}{2}\right)\right],\ \ \hat{\lambda}_{\pm 3}(r) = \pm\frac{i}{2}\,\mathrm{sech}\left(\frac{r}{4}\right)\ .$$

The Melnikov function can be exactly obtained from Proposition 2.1 to be

$$M(t) = 2\,[\mathrm{sech}\,(\pi) + \mathrm{cosech}\,(\pi)]\cos(4\,\pi t) - \mathrm{sech}\left(\frac{3\,\pi}{2}\right)\sin(6\pi t)\ .$$

There are four roots to the equation $M(t) = 0$ in the fundamental domain $[0, 1)$; Mathematica was used to determine these with 30 digits of accuracy. These roots are very close to being equally spaced; two of the subintervals created have lengths 0.249678 (to six digit accuracy), whereas the other two have lengths 0.256180 and 0.244463 (greater accuracy is available and was used in the calculations). A straightforward application of Theorem 4.1 gives the value $s = 0.2202363444$.

6.7. Case (vii). A much more general instance is now examined, in which h is not separable, and there are infinitely many terms in its Fourier expansion. Suppose that $h^x(x,y,t) = w(2x-2y-t)$, where w is the 2-periodic triangular wave given in its base domain by

$$w(\xi) = \begin{cases} \frac{1}{2} + \xi & \text{if} \quad -1 \le \xi < 0, \\ \frac{1}{2} - \xi & \text{if} \quad 0 < \xi \le 1. \end{cases}$$

The perturbation corresponds to a diagonally traveling triangular wave. Utilizing the Fourier expansion for $w(\xi)$, it is possible to represent $h^x(x,y,t)$ by

$$h^x(x,y,t) = w(2x-2y-t) = \sum_{n=-\infty,\text{odd}}^{\infty} \frac{2}{n^2\,\pi^2} \exp\left[in\pi 2(x-y)\right] \exp\left[in\pi t\right],$$

from which the x-components of the g_n functions for odd n can be expressed as

$$g_n^x(x,y) = \frac{2}{n^2\,\pi^2} \exp\left[-i\,2\,\pi\,n\,(x-y)\right].$$

The corresponding functions $\lambda_n(t)$ are zero for even n and for odd n turn out to be

$$\lambda_n(t) = \frac{2}{n^2\,\pi^2} \left(\cos\left[2\,\pi\,n\,\bar{y}(t)\right] + i\,\sin\left[2\,\pi\,n\,\bar{y}(t)\right]\right),$$

which satisfy $\lambda_{-n} = \lambda_n^*$. Given that $\lambda_n(t)$'s real part is even in t and its imaginary part is odd, its Fourier transform $\hat{\lambda}_n(r)$ is purely real. Moreover, the Fourier coefficients d_n of the Melnikov function satisfy $d_n = \hat{\lambda}_n(n\,\pi)$, which are therefore themselves real. Furthermore,

$$d_{-n} = \hat{\lambda}_{-n}(-n\pi) = \int_{-\infty}^{\infty} e^{-i(-n\pi)t} \lambda_{-n}(t)\,\mathrm{d}t = \left[\int_{-\infty}^{\infty} e^{-in\pi t} \lambda_n(t)\,\mathrm{d}t\right]^* = d_n^*,$$

and hence $d_{-n} = d_n$ as well. The Melnikov function is therefore

$$M(t) = 2 \sum_{m=1}^{\infty} d_{2m-1} \cos\left[(2m-1)\,\pi t\right]. \tag{6.2}$$

The computation of the d_n's turns out to be possible *explicitly* for any given positive integer n. From the relationship $\cos\left[2\pi\bar{y}(t)\right] = -\,\mathrm{sech}\,(2\pi t)$ it is possible to generate the recurrence relation

$$\begin{pmatrix} \cos\left[(n+1)2\pi\bar{y}(t)\right] \\ \sin\left[(n+1)2\pi\bar{y}(t)\right] \end{pmatrix} = \begin{pmatrix} -\,\mathrm{sech}\,(2\pi t) & \tanh\,(2\pi t) \\ -\tanh\,(2\pi t) & -\,\mathrm{sech}\,(2\pi t) \end{pmatrix} \begin{pmatrix} \cos\left[n2\pi\bar{y}(t)\right] \\ \sin\left[n2\pi\bar{y}(t)\right] \end{pmatrix},$$

from which for positive integer n the result

$$\begin{pmatrix} \cos\left[2\,\pi\,n\,\bar{y}(t)\right] \\ \sin\left[2\,\pi\,n\,\bar{y}(t)\right] \end{pmatrix} = \begin{pmatrix} -\,\mathrm{sech}\,(2\pi t) & \tanh\,(2\pi t) \\ -\tanh\,(2\pi t) & -\,\mathrm{sech}\,(2\pi t) \end{pmatrix}^{n-1} \begin{pmatrix} -\,\mathrm{sech}\,(2\pi t) \\ -\tanh\,(2\pi t) \end{pmatrix}$$

can be obtained. Thus, the real and imaginary parts of $\lambda_n(t)$ can be computed for any positive integer n. It turns out that the Fourier transform of $\lambda_n(t)$ is also explicitly computable in

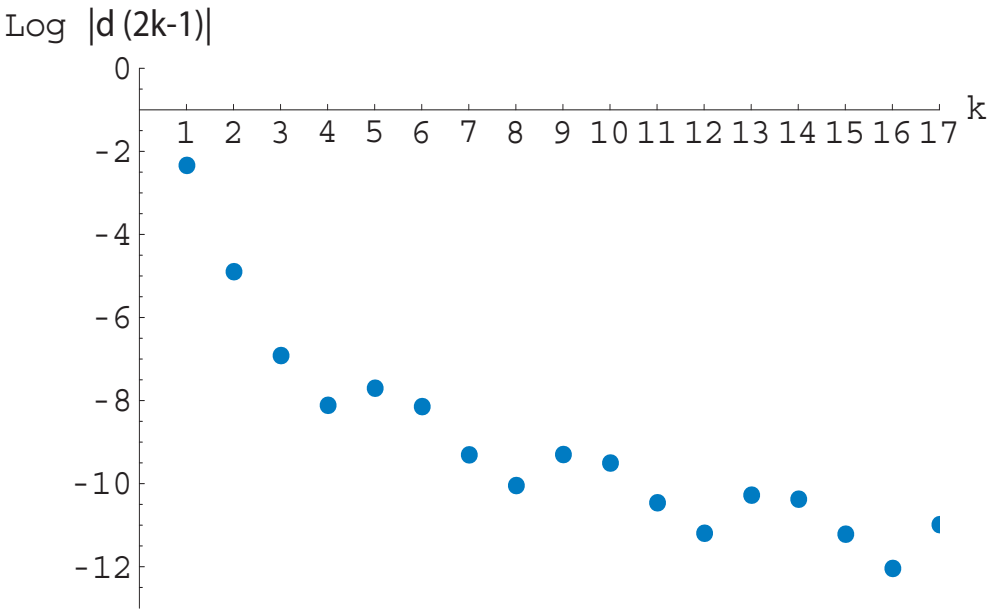

Figure 6.7. *The slow decay of the Fourier coefficients of the Melnikov function illustrated in a semi-log graph for case* (vii).

terms of exponential functions for any positive integer n, and hence d_n can be determined for any n. A Mathematica routine performing this task is provided with the supplementary material for this article. It computes, for example,

$$d_{33} = -\frac{92717622204276507853284597169\,\exp(99\,\pi/4)}{3080690429637219581952\,[\exp(33\,\pi)-1]\,\pi^2} \approx -1.69\times 10^{-5}\,,$$

and higher-order terms take significant computational time. Figure 6.7 illustrates the decay of the $|d_{2m-1}|$ in a semi-log graph. Unlike in earlier examples, the decay is nonmonotone, and it is also slow (d_{33} as expressed above is still of order 10^{-5}). Nevertheless, the Melnikov function computed from (6.2) appears to the naked eye to converge rapidly with the inclusion of only a few terms. It is indeed qualitatively similar to *negative* the Melnikov function of case (ii) (pictured in Figure 6.4). It is clear from (6.2) that it has zeros at $t = 1/2$ and $t = 3/2$, and the numerically computed graph indicates that these are the only zeros in the base domain.

Since the zeros of M are equally spaced, it is possible to use Proposition 4.5 to compute the chaotic flux. The Melnikov function is almost in the correct form for direct application of its result, the only shortcoming being that the subinterval centered at $t = 0$ corresponds to a negative M. This can be compensated for in the result of Proposition 4.5 by the simple stratagem of including an additional negative sign, leading to the formula

$$s = \lim_{N\to\infty} \frac{4}{\pi} \sum_{m=1}^{N} \frac{(-1)^m\, d_{2m-1}}{2m-1} =: \lim_{N\to\infty} s(N)\,.$$

The nonrapid convergence of the d_ns results in $s(N)$ having relatively slow convergence, to a value which appears to be 0.120048 correct to six significant figures. The fact that exact

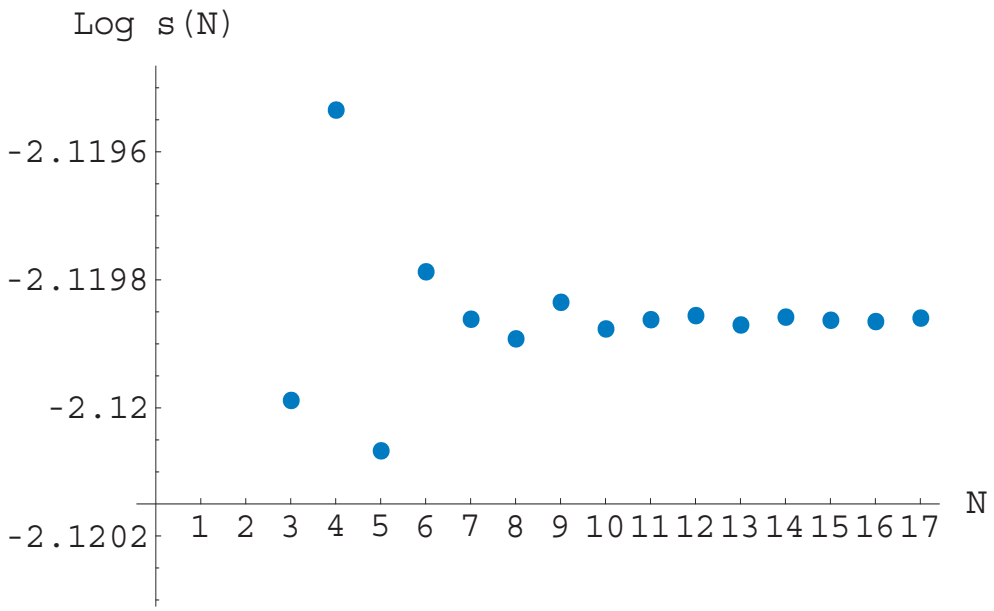

Figure 6.8. *The convergence of* $s(N)$ *for case* (vii) *in a semi-log plot.*

expressions are available for the d_ns make each computation of $s(N)$ correct to a very high degree of accuracy; twenty significant digits were used in the present calculations. The convergence behavior of $s(N)$ is illustrated in Figure 6.8, again using a semi-log graph to accentuate the differences. Using only three nonzero terms in the summation gives a good approximation immediately (to about two significant figures), but obtaining a very refined value for the flux requires more numerical effort because of the slow, apparently oscillatory, convergence.

7. Concluding remarks. The available leading-order chaotic flux formula for separable harmonic perturbations [6, 7] has been extended to nonseparable, general periodic, perturbations. This is a direct assessment of the chaotic flux crossing a separatrix in the sense that it comes from a direct computation of the area transported per unit time. The formulae were obtained through a procedure which involved computation of the Fourier coefficients of the Melnikov function, which was accomplished through appropriate Fourier transforms. Knowledge of the distribution of zeros of the Melnikov function then leads to a relatively simple formula for the flux, involving bi-infinite summations over modulated Fourier coefficients. Several results were presented for special cases, such as when the zeros were evenly distributed, when the perturbation was separable, and also when its temporal part was harmonic modulo a shift. The directional leading-order fluxes were also computed using the theory.

An example was analyzed in detail, with seven different perturbations used. It was seen that the flux computations were particularly easy in the separable instance, since in this case only *one* Fourier transform needs to be computed. In the more general case, the calculations may not be as easy. In many cases, however, the bi-infinite series for the flux was usually seen to converge quite rapidly in a gross sense. Chaotic flux quantification was achieved for significantly nontrivial perturbations of this planar cellular flow. Calculations were possi-

ble using a naive implementation of Mathematica, without requiring sophisticated numerical techniques which would normally be needed if attempting to compute lobe areas directly. It is expected that this algorithm for computing the leading-order chaotic flux would be viable in substantially more complicated instances than the illustrative example of section 6. While more thought may be required in the numerical details, the accessibility of Fourier transform software renders this approach particularly attractive.

REFERENCES

[1] S. S. Abdullaev, *Structure of motion near saddle points and chaotic transport in Hamiltonian systems*, Phys. Rev. E (3), 62 (2000), pp. 3508–3528.

[2] A. Adrover, M. Giona, F. J. Muzzio, S. Cerbelli, and M. M. Alvarez, *Analytic expression for the short-time rate of growth of the intermaterial contact parameter in two-dimensional chaotic flows and Hamiltonian systems*, Phys. Rev. E (3), 58 (1998), pp. 447–457.

[3] T. Ahn and S. Kim, *Separatrix-map analysis of chaotic transport in planar periodic vortical flows*, Phys. Rev. E (3), 49 (1994), pp. 2900–2912.

[4] D. K. Arrowsmith and C. M. Place, *An Introduction to Dynamical Systems*, Cambridge University Press, Cambridge, UK, 1990.

[5] P. Ashwin, M. Nicol, and N. Kirkby, *Acceleration of one-dimensional mixing by discontinuous mappings*, Phys. A, 310 (2002), pp. 347–363.

[6] S. Balasuriya, *Optimal perturbation for enhanced chaotic transport*, Phys. D, accepted, 2004.

[7] S. Balasuriya, *Chaotic flux generated through time-periodic forcing of Euler flows*, Eurupean J. Appl. Math., submitted, 2004.

[8] S. Balasuriya, *Non-exponentially small separatrix splitting under high frequency perturbations*, Discrete Contin. Dynam. Systems, submitted, 2004.

[9] S. Balasuriya and C. K. R. T. Jones, *Diffusive draining and growth of eddies*, Nonlin. Proc. Geophys., 8 (2001), pp. 241–251.

[10] S. Balasuriya, C. K. R. T. Jones, and B. Sandstede, *Viscous perturbations of vorticity-conserving flows and separatrix splitting*, Nonlinearity, 11 (1998), pp. 47–77.

[11] S. Balasuriya, I. Mezić, and C. K. R. T. Jones, *Weak finite-time Melnikov theory and 3D viscous perturbations of Euler flows*, Phys. D, 176 (2003), pp. 82–106.

[12] D. Beigie, A. Leonard, and S. Wiggins, *Chaotic transport in the homoclinic and heteroclinic tangle regions of quasiperiodically forced two-dimensional dynamical systems*, Nonlinearity, 4 (1991), pp. 775–819.

[13] S. Chandrasekhar, *Hydrodynamics and Hydrodynamic Stability*, Dover, New York, 1961.

[14] L. Chierchia and G. Gallavotti, *Drift and diffusion in phase space*, Ann. Inst. H. Poincaré Physique Theorique, 60 (1994), pp. 1–144.

[15] B. V. Chirikov, *A universal instability of many-dimensional oscillator systems*, Phys. Rep., 52 (1979), pp. 263–379.

[16] B. V. Chirikov and V. V. Vecheslavov, *Arnold diffusion in large systems*, J. Exp. Theor. Phys., 85 (1997), pp. 616–624.

[17] D. D'Alessandro, M. Dahleh, and I. Mezić, *Control of mixing in fluid flow: A maximum entropy approach*, IEEE Trans. Automat. Control, 44 (1999), pp. 1852–1863.

[18] A. Delshams and T. M. Seara, *Splitting of separatrices in Hamiltonian systems with one and a half degrees of freedom*, Math. Phys. Electron. J., 3 (1997), Paper 4, 40 pp.

[19] M. Giona, A. Adrover, F. J. Muzzio, S. Cerbelli, and M. M. Alvarez, *The geometry of mixing in time-periodic chaotic flows. I. Asymptotic directionality in physically realizable flows and global invariant properties*, Phys. D, 132 (1999), pp. 298–324.

[20] J. Guckenheimer and P. Holmes, *Nonlinear Oscillations, Dynamical Systems and Bifurcations of Vector Fields*, Springer-Verlag, New York, 1983.

[21] T. J. Kaper and S. Wiggins, *Lobe area in adiabatic systems*, Phys. D, 51 (1991), pp. 205–212.

[22] R. S. MacKay, J. D. Meiss, and I. C. Percival, *Transport in Hamiltonian systems*, Phys. D, 13 (1984), pp. 55–81.
[23] J. D. Meiss, *Symplectic maps, variational principles, and transport*, Rev. Modern Phys., 64 (1992), pp. 795–847.
[24] J. M. Ottino, *Mixing, chaotic advection, and turbulence*, in Annual Review of Fluid Mechanics, Annu. Rev. Fluid Mech. 22, Annual Reviews, Palo Alto, CA, pp. 207–253.
[25] V. Rom-Kedar, *Transport rates of a class of two-dimensional maps and flows*, Phys. D, 43 (1990), pp. 229–268.
[26] V. Rom-Kedar, *Homoclinic tangles—classification and applications*, Nonlinearity, 7 (1994), pp. 441–473.
[27] V. Rom-Kedar, *Secondary homoclinic bifurcation theorems*, Chaos, 5 (1995), pp. 385–401.
[28] V. Rom-Kedar, *Frequency spanning homoclinic families*, Commun. Nonlinear Sci. Numer. Simul., 8 (2003), pp. 149–169.
[29] V. Rom-Kedar, A. Leonard, and S. Wiggins, *An analytical study of transport, mixing and chaos in an unsteady vortical flow*, J. Fluid Mech., 214 (1990), pp. 347–394.
[30] V. Rom-Kedar and A. C. Poje, *Universal properties of chaotic transport in the presence of diffusion*, Phys. Fluids, 11 (1999), pp. 2044–2057.
[31] V. Rom-Kedar and S. Wiggins, *Transport in two-dimensional maps*, Arch. Ration. Mech. Anal., 109 (1990), pp. 239–298.
[32] B. Sandstede, S. Balasuriya, C. K. R. T. Jones, and P. Miller, *Melnikov theory for finite-time vector fields*, Nonlinearity, 13 (2000), pp. 1357–1377.
[33] B. I. Shraiman, *Diffusive transport in a Rayleigh-Bénard convection cell*, Phys. Rev. A (3), 36 (1987), pp. 261–267.
[34] T. H. Solomon and J. P. Gollub, *Chaotic particle transport in time-dependent Rayleigh-Bénard convection*, Phys. Rev. A (3), 38 (1988), pp. 6280–6286.
[35] S. Wiggins, *Chaotic Transport in Dynamical Systems*, Springer-Verlag, New York, 1992.